applied sciences

MDPI

Article

Interleaved Boost Converter with ZVT-ZCT for the Main Switches and ZCS for the Auxiliary Switch

Kuo-Ing Hwu [1,*], Jenn-Jong Shieh [2,*] and Wen-Zhuang Jiang [3,*]

1 Department of Electrical Engineering, National Taipei University of Technology, 1, Sec. 3, Zhongxiao E. Rd., Taipei 10608, Taiwan
2 Department of Electrical Engineering, Feng Chia University, No. 100, Wenhwa Road, Seatwen, Taichung 40724, Taiwan
3 Chicony Power Technology Co., Ltd., Sanchong, New Taipei 24158, Taiwan
* Correspondence: eaglehwu@ntut.edu.tw (K.-I.H.); jjshieh@fcu.edu.tw (J.-J.S.); Vincent_Jiang@chiconypower.com.tw (W.-Z.J.); Tel.: +886-2-27712171 (ext. 2159) (K.-I.H.); +886-4-24517250 (ext. 3815) (J.-J.S.); +886-2-66260678 (ext. 52281) (W.-Z.J.)

Received: 17 February 2020; Accepted: 10 March 2020; Published: 17 March 2020

check for updates

Abstract: A soft-switching interleaved topology is presented herein and applied to the boost converter. The basic operating principle is that the main power switches are turned on at zero voltage and turned off at zero current via the same auxiliary resonant circuit whose switch is turned on from zero current. Furthermore, as compared to the traditional boost converter, the proposed topology has three additional auxiliary diodes, two additional auxiliary capacitors, one additional auxiliary inductor, and one additional auxiliary switch. On the other hand, since the interleaved control is adopted herein, the difference in current between the two phases exists. Hence, the cascaded control is utilized to regulate the output voltage to the desired voltage via the first phase, whereas the current-sharing control, based on half of the input current as the current reference for the second phase, is employed so as to make the load current extracted from the two phases as evenly as possible. In this paper, the effectiveness of the proposed topology and control strategy is demonstrated by some experimental results.

Keywords: boost converter; soft switching; zero voltage transition; zero current transition; zero current switching; cascaded control; interleaved control

1. Introduction

Generally, the traditional switching power supply operates under hard switching. However, due to the parasitic components, large electromagnetic interference and high switching loss will happen the instant the switch is turned on/off. Accordingly, the soft switching concept is presented [1–5]. Based on an auxiliary inductor connected in series with the switch, this inductor will oscillate with the parasitic capacitor during the turn-off period, and, as soon as the voltage across the parasitic capacitor resonates to zero, the switch will be turned on. This behavior is called zero-voltage switching (ZVS) at turn-on. Moreover, as soon as the current in the auxiliary inductor resonates to zero, the switch will be turned off. This behavior is called zero-current switching (ZCS) at turn-off. However, although the switching loss is reduced based on ZVS or ZCS or both, high resonant voltage stress or high resonant current stress is generated so as to select proper components, thereby increasing the corresponding circuit cost. In addition, since the turn-on and turn-off intervals are determined by the resonant period, the variable-frequency control is chosen so as to stabilize the output voltage, thereby making the filter design difficult.

As seen in the half-resonant drawbacks, the active clamp [6–30], the zero-voltage transition (ZVT) [21–27] and the zero-current transition (ZCT) [28–30] are presented. As the voltage clamp is applied to the non-isolated power supply, the parasitic inductance of the line and the leakage inductance of the transformer are used as the auxiliary inductance, which will oscillate with the auxiliary capacitance. Via this way, the switch can reach soft switching during the resonant period. As the auxiliary switch is turned off, the current in the auxiliary inductance flows through the input terminals, thereby making the body diode of the main switch turn on, and hence the main switch has soft switching and the energy stored in the auxiliary inductance is transferred to the input terminals. By doing so, the overall efficiency is increased. As the active clamp technique is applied to the non-isolated power converter [31], one auxiliary inductance, one auxiliary capacitance, and one auxiliary switch are used to form a resonant loop, and, during the resonant period, the soft switching of the main switch and auxiliary switch can be achieved. Via this way, the voltage stress on the main switch is reduced in addition to the switching loss. However, the switching frequency is varied according to output load and input voltage, and an auxiliary inductance is inserted in the power path. Consequently, although the soft switching of the main switch can be achieved, the low-pass filter is designed difficultly, and the conduction loss is severe as this converter operates under the half or rated load.

As the ZVT or ZCT technique is applied to the power supply, one auxiliary resonant circuit is connected in parallel with the main switch. Before the main switch is turned on or off, the auxiliary switch is turned on and hence the resonance occurs, forcing the voltage on the main switch or the current in the main switch to be zero. Since the resonance circuit does not locate in the main power path, the conduction loss is reduced and hence the overall efficiency is increased. The literatures [32–34] employ ZVT and ZCT simultaneously, so that the switching loss can be reduced and hence the overall efficiency can be enhanced.

On the one hand, in order to upgrade the output current as well as to improve the efficiency, the multiphase converter, along with interleave control, is widely used. The fact that the AC components of the inductor currents for multiple phases are cancelled to some extent makes the output current ripple reduce as well as the frequency of the output current ripple increase. By doing so, the required filter design will be easier and the corresponding size will be smaller. In general, the total loss created from multiple phases will be smaller than that created from a single phase. Accordingly, the multiphase converter with soft switching is presented. The literatures [33–36] adopt multiple phases with the corresponding number of auxiliary resonance circuits, leading to increasing the number of components to increase conduction loss as well as cost. In the literature [35], the two-phase converter uses the same auxiliary resonant circuit. However, only the ZVS is used, such that the efficiency improvement is limited. In the literature [36], the two-phase converter uses one snubber circuit so as to make the main switches achieve soft switching. However, the resonant inductor locates in the power path, thereby making conduction loss increased.

On the other hand, there are differences in component features and line impedance between the two phases. Consequently, the current-sharing control will be needed. As for current sharing, there are two types of current-sharing control methods. One is passive; the other is active. The former employs capacitors or differential-mode transformers or both to do current sharing [37–40], whereas the latter contains current regulators and current sensors to balance currents [41–45].

Based on what has been discussed above, a two-phase converter with one resonant inductor, two resonant capacitors, two resonant diodes, one auxiliary diode, one auxiliary switch, and two main switches are proposed. This converter can achieve ZVT and ZCT for the main switches and ZCS for the auxiliary switch, so as to further increase the overall efficiency. In addition, the proposed current-sharing control is adopted herein so that the output voltage is regulated by the first phase and the current sharing between the two phases is controlled by the second phase.

2. Two-Phase Converter with Proposed Soft Switching

In Figure 1, the proposed inductor resonant circuit applied to the two-phase interleaved converter is built up by only one resonant L_r, two resonant capacitors C_{r1} and C_{r2}, two resonant diodes D_{r1} and D_{r2}, one auxiliary switch S_a, and one auxiliary diode D_a.

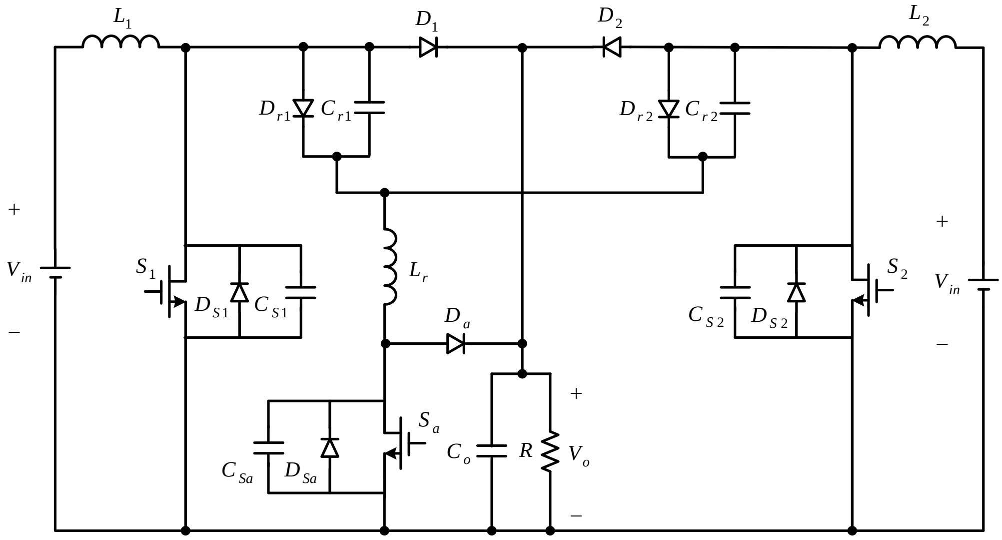

Figure 1. Proposed soft-switching interleaved boost converter.

3. Basic Operating Principles

Prior to the circuit analysis, there are some assumptions as below: (i) all the main switches and diodes are viewed as ideal; (ii) no parasitic resistances exist in the inductor and capacitors; (iii) the ideal input inductor can be considered as current source such that L_1, L_2, and V_{in} can be removed.; (iv) the ideal output capacitor can be regarded as a voltage source such that C_o and R_o can be removed. Based on the above, the circuit in Figure 2 is an equivalent circuit for Figure 1. In Figure 3, there are twenty-two operating states. Since this converter is controlled by interleave, the behavior of the first eleven states is the same as that of the last eleven states. Therefore, only the first eleven states are described.

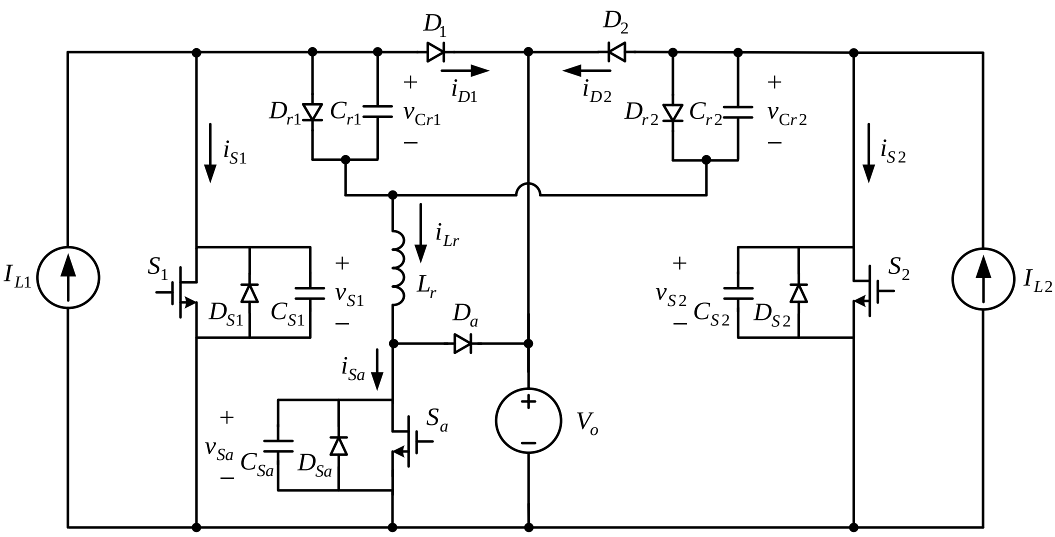

Figure 2. Equivalent circuit of the circuit shown in Figure 1.

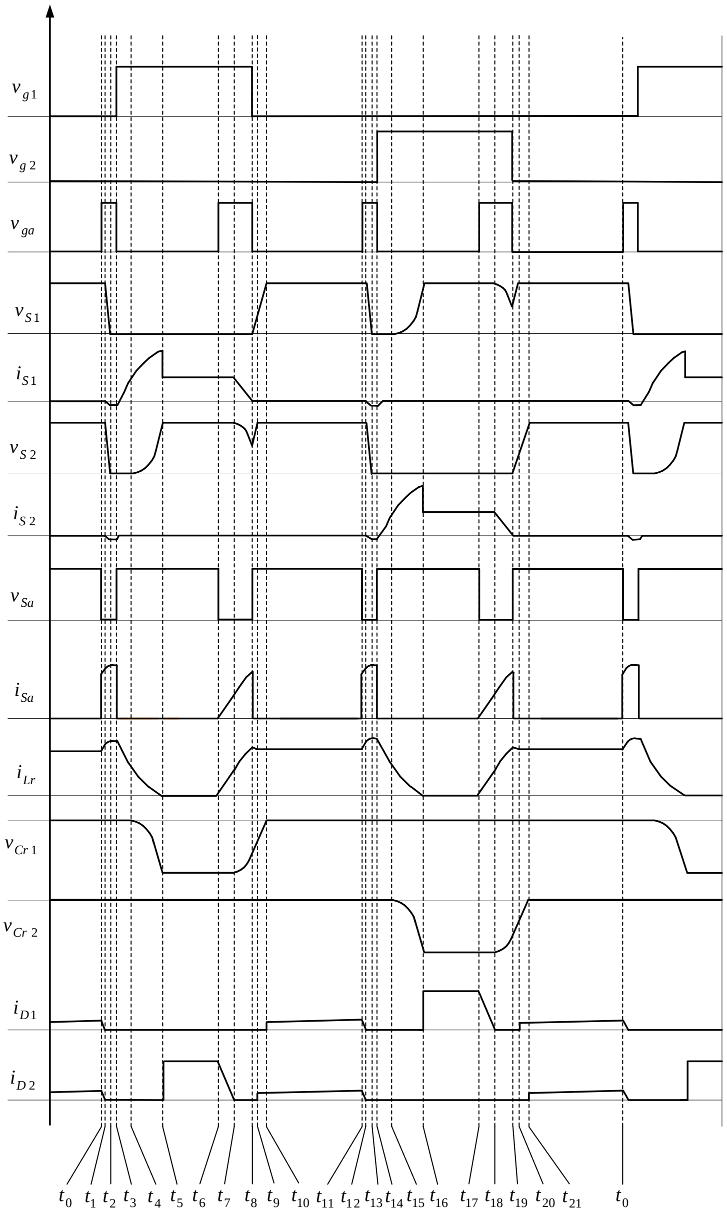

Figure 3. Illustrated waveforms for the proposed converter.

State 1: $[t_0 \le t \le t_1]$. As shown in Figure 4, the main switches S_1 and S_2 are turned off but the auxiliary switch S_a is turned on, whereas the freewheeling diodes D_1 and D_2 as well as the resonant diodes D_{r1} and D_{r2} are turned on. During this state, the resonant inductor L_r is magnetized, and hence the resonant inductor current i_{Lr} is linearly increased. In addition, the energy required by the load is provided by the current I_L, which is equal to the current I_{L1} plus the current I_{L2}. As soon as i_{Lr} is equal to I_L, D_1 and D_2 are turned off, and hence this state comes to the end. During this interval, the corresponding state equation can be expressed as follows:

$$i_{Lr}(t) = \frac{V_o}{L_r}(t - t_0) + i_{Lr}(t_0) \tag{1}$$

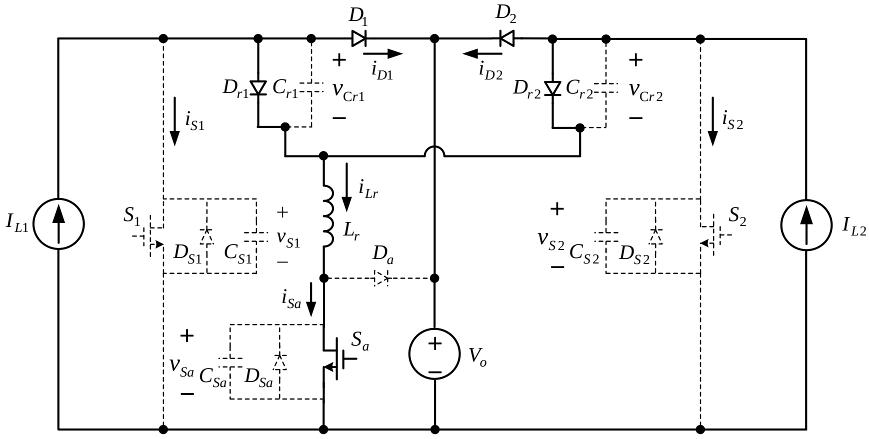

Figure 4. Current flow in state 1.

As $t = t_1$, $i_{Lr}(t_1) = I_L$, and hence the corresponding time elapsed is as follows:

$$(t_1 - t_0) = \frac{[I_L - i_{Lr}(t_0)]L_r}{V_o} \tag{2}$$

State 2: $[t_1 \le t \le t_2]$. As shown in Figure 5, the main switches S_1 and S_2 are still turned off but the auxiliary switch S_a is still turned on, whereas the freewheeling diodes D_1 and D_2 are turned off but the resonant diodes D_{r1} and D_{r2} are still turned on. During this state, the parasitic capacitors of S_1 and S_2, called C_{S1} and C_{S2}, resonate with the resonant inductor L_r, thereby making the resonant inductor current i_{Lr} keep increasing. In addition, the output capacitor C_o provides energy to the load. The moment C_{S1} and C_{S2} are discharged to zero, the parasitic diodes of the main switches S_1 and S_2, called D_{S1} and D_{S2}, are turned on, and hence this state comes to the end. During this interval, the corresponding state equation can be represented as follows:

$$\begin{cases} i_{Lr}(t) = I_L + \frac{v_S(t_1)}{Z_2}\sin\omega_2(t-t_1) - [I_L - i_{Lr}(t_1)]\cos\omega_2(t-t_1) \\ v_S(t) = Z_2[I_L - i_{Lr}(t_1)]\sin\omega_2(t-t_1) + v_S(t_1)\cos\omega_2(t-t_1) \end{cases} \tag{3}$$

where

$$\omega_2 = \sqrt{\frac{1}{L_r C_S}},\ Z_2 = \sqrt{\frac{L_r}{C_S}},\ C_S = C_{S1} + C_{S2} \text{ and } v_{S1} = v_{S2} = v_S \tag{4}$$

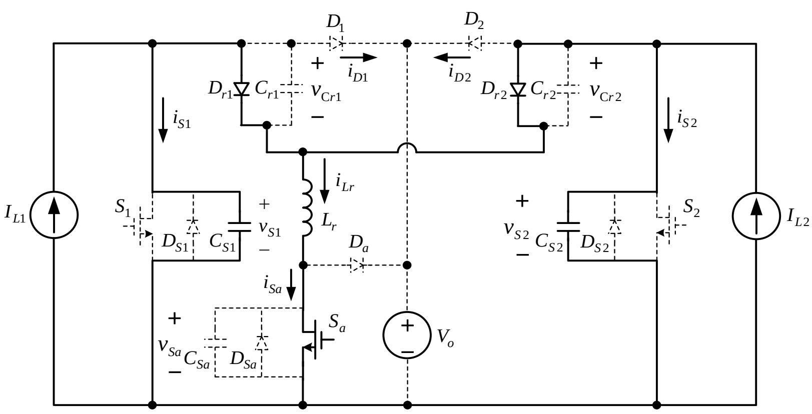

Figure 5. Current flow in state 2.

And hence, the corresponding time elapsed is as follows:

$$(t_2 - t_1) = \frac{\pi}{2\omega_2} \tag{5}$$

State 3: $[t_2 \le t \le t_3]$. As shown in Figure 6, the main switches S_1 and S_2 are still turned off but the auxiliary switch S_a is still turned on, whereas the freewheeling diodes D_1 and D_2 are still turned off but the resonant diodes D_{r1} and D_{r2} are still turned on. During this state, the parasitic diodes of the main switches S_1 and S_2, called D_{S1} and D_{S2}, are turned on, and hence the voltages across S_1 and S_2, called v_{s1} and v_{s2}, are zero. In addition, the output capacitor C_o still provides energy to the load. The instant the auxiliary switch S_a is turned off, S_1 has zero-voltage-transition (ZVT) turn-on and hence this state comes to the end. During this interval, the corresponding state equation can be signified as follows:

$$i_{Lr}(t) = I_L + \frac{V_o}{Z_2} \tag{6}$$

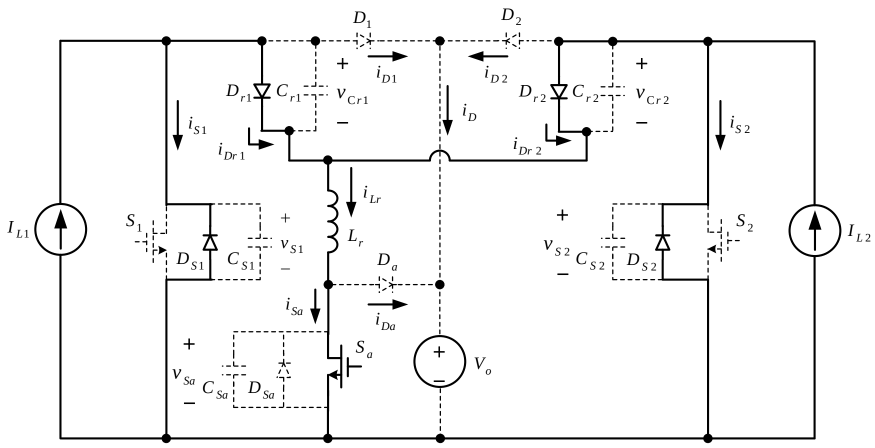

Figure 6. Current flow in state 3.

State 4: $[t_3 \le t \le t_4]$. As shown in Figure 7, the main switch S_1 is turned on but the main switch S_2 is still turned off and the auxiliary switch S_a is turned off, whereas the freewheeling diodes D_1 and D_2 are still turned off but the resonant diodes D_{r1} and D_{r2} are still turned on. During this state, the current i_{S1} begins to increase, and the auxiliary diode D_a is turned on due to S_a being turned off, thereby making the voltage across the resonant inductor L_r change its polarity such that L_r is demagnetized. Once $i_{S1} = I_{L1}$ and $i_{Lr} = I_{L2}$, the resonant diode D_{r1} is turned off, and hence this state comes to the end. During this interval, the corresponding state equation can be represented as follows:

$$i_{Lr}(t) = \frac{-V_o}{L_r}(t - t_3) + I_L + \frac{V_o}{Z_2} \tag{7}$$

As $t = t_4$, the corresponding time elapsed is as follows:

$$(t_4 - t_3) = \frac{[I_L + \frac{V_o}{Z_2} - i_{Lr}(t_4)]L_r}{V_o} \tag{8}$$

State 5: $[t_4 \le t \le t_5]$. As shown in Figure 8, the main switch S_1 is still turned on but the main switch S_2 is still turned off and the auxiliary switch S_a is still turned off, whereas the freewheeling diodes D_1 and D_2 are still turned off and the resonant diode D_{r1} is turned off but the resonant diode D_{r2} is still turned on. During this state, the inductor current I_{L2} charges the parasitic capacitor of the main switch S_2, called C_{S2}, and also charges the resonant capacitor C_{r1} in the opposite direction.

At the same time, the resonant inductor L_r still keeps demagnetized, and as the resonant current i_{Lr} is deceased to zero, the voltage across C_{S2}, called v_{S2}, is increased to the output voltage V_o and the voltage across C_{r1}, called v_{Cr1}, is decreased to $-V_o$. The moment the auxiliary diode D_a is turned off, the freewheeling diode D_2 is turned on, and hence this state comes to the end. During this interval, the corresponding state equation can be signified as follows:

$$\begin{cases} i_{Lr}(t) = I_{L2} + \frac{v_A(t_4) - V_o}{Z_5} \sin \omega_5 (t - t_4) - [I_{L2} - i_{Lr}(t_4)] \cos \omega_5 (t - t_4) \\ v_A(t) = V_o + Z_5 [I_{L2} - i_{Lr}(t_4)] \sin \omega_5 (t - t_4) + [v_A(t_4) - V_o] \cos \omega_5 (t - t_4) \end{cases} \tag{9}$$

where v_A is the voltage across C_A, and

$$C_A = C_{r1} + C_{S2}, \omega_5 = \sqrt{\frac{1}{L_r C_A}} \text{ and } Z_5 = \sqrt{\frac{L_r}{C_A}} \tag{10}$$

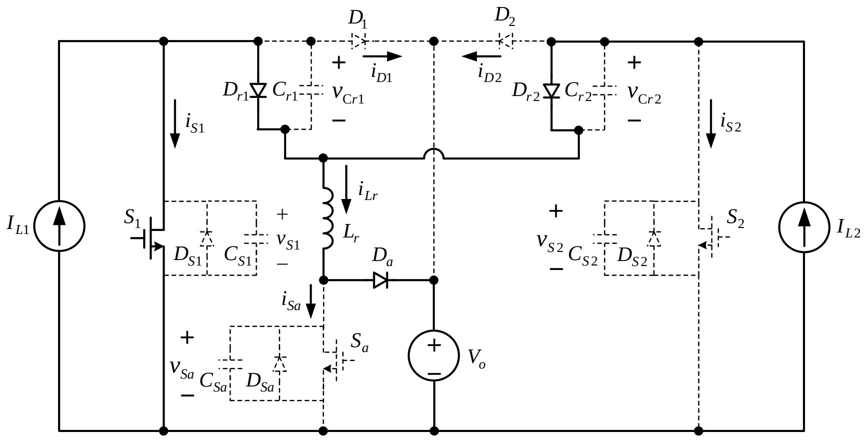

Figure 7. Current flow in state 4.

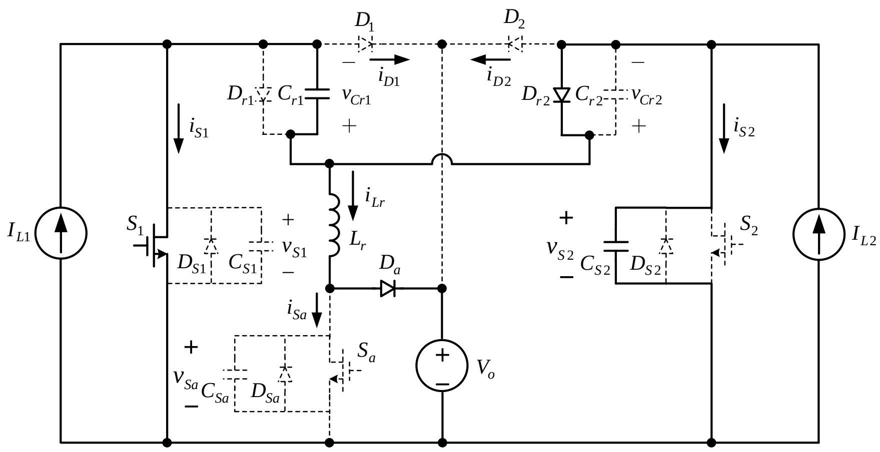

Figure 8. Current flow in state 5.

Hence, the corresponding time elapsed is as follows:

$$(t_5 - t_4) = \frac{\pi}{2\omega_5} \tag{11}$$

State 6: $[t_5 \le t \le t_6]$. As shown in Figure 9, the main switch S_1 is still turned on but the main switch S_2 is still turned off and the auxiliary switch S_a is still turned off, whereas the freewheeling diode D_1 is still turned off but the freewheeling diode D_2 is turned on but the resonant diode D_{r1} is still turned off and the resonant diode D_{r2} is turned off. During this state, the operating behavior of this converter is the same as that of the traditional boost converter. The instant D_{r2} and S_a are both turned on, this state comes to the end. At the same time, since S_a is connected in series with the resonant inductor L_r, the current flowing through S_a, called i_{Sa}, is slowly increased from zero, making S_a turned on with zero current switching (ZCS).

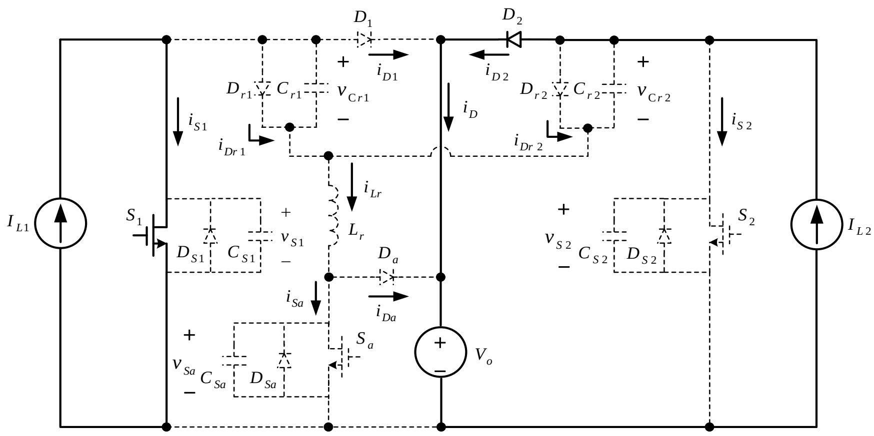

Figure 9. Current flow in state 6.

State 7: $[t_6 \leq t \leq t_7]$. As shown in Figure 10, the main switch S_1 is still turned on but the main switch S_2 is still turned off but the auxiliary switch S_a is turned on, whereas the freewheeling diode D_1 is still turned off but the freewheeling diode D_2 is still turned on but the resonant diode D_{r1} is still turned off but the resonant diode D_{r2} is turned on. During this state, since S_a and D_{r2} are turned on, the resonant inductor L_r is to be magnetized. Once $i_{Lr} = I_{L2}$, this state comes to the end. During this interval, the corresponding state equation can be expressed as follows:

$$i_{Lr}(t) = \frac{V_o}{L_r}(t - t_6) + i_{Lr}(t_6) \tag{12}$$

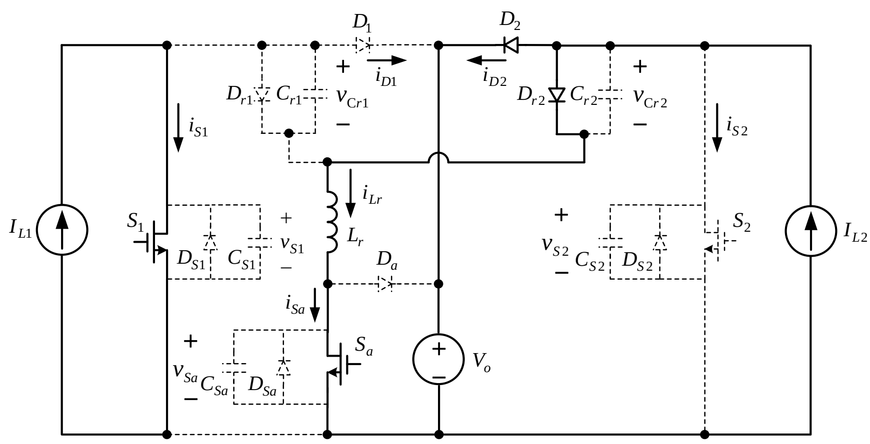

Figure 10. Current flow in state 7.

As $t = t_6$, $i_{Lr}(t_6) = 0$, whereas as $t = t_7$, $i_{Lr}(t_7) = I_{L2}$. Accordingly, the corresponding time elapsed is

$$(t_7 - t_6) = \frac{I_{L2}L_r}{V_o} \tag{13}$$

State 8: $[t_7 \le t \le t_8]$. As shown in Figure 11, the main switch S_1 is still turned on but the main switch S_2 is still turned off but the auxiliary switch S_a is still turned on, whereas the freewheeling diodes D_1 and D_2 are turned off and the resonant diode D_{r1} is still turned off but the resonant diode D_{r2} is still turned on. During this state, the resonant capacitor C_{r1} and the parasitic capacitor C_{S2} of the main switch S_2 resonate with the resonant inductor L_r. Therefore, C_{S2} is discharged, C_{r1} is discharged in the opposite direction, and the resonant inductor remains demagnetized. In addition, the output capacitor C_o provides energy to the load. As soon as the current in S_1 is decreased to zero, S_1 is turned off with zero current transition (ZCT) and hence this state comes to the end. During this interval, the corresponding state equation can be represented as follows:

$$\begin{cases} i_{Lr}(t) = I_{L2} + \frac{v_A(t_7)}{Z_8}\sin\omega_8(t-t_7) - [I_{L2} - i_{Lr}(t_7)]\cos\omega_8(t-t_7) \\ v_A(t) = Z_8[I_{L2} - i_{Lr}(t_7)]\sin\omega_8(t-t_7) + v_A(t_7)\cos\omega_8(t-t_7) \end{cases} \tag{14}$$

where

$$\omega_8 = \sqrt{\frac{1}{L_rC_A}} \text{ and } Z_8 = \sqrt{\frac{L_r}{C_A}} \tag{15}$$

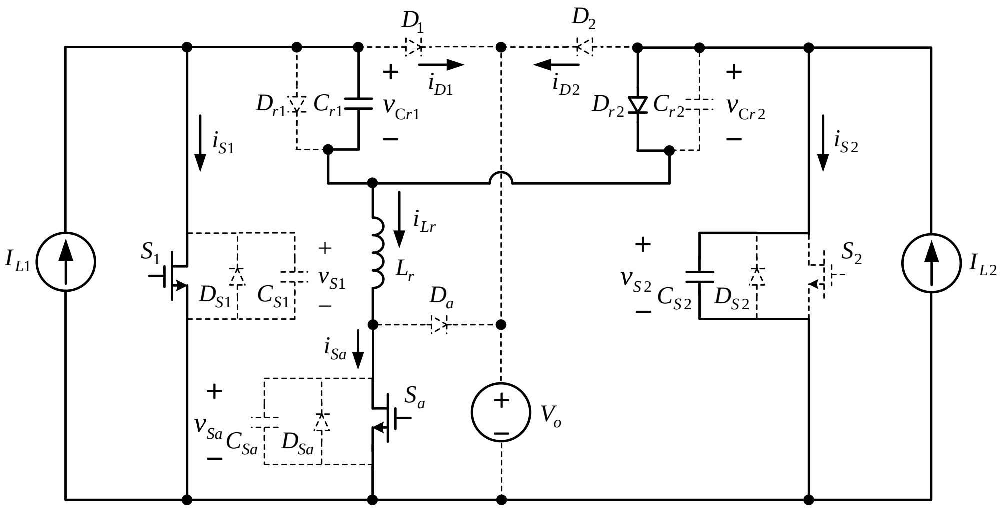

Figure 11. Current flow in state 8.

Accordingly, the corresponding time elapsed is as follows:

$$(t_8 - t_7) = \frac{1}{\omega_8}\sin^{-1}\left(\frac{[i_{Lr}(t_8) - I_{L2}]Z_8}{V_o}\right) \tag{16}$$

State 9: $[t_8 \le t \le t_9]$. As shown in Figure 12, the main switch S_1 is turned off and the main switch S_2 is still turned off and the auxiliary switch S_a is turned off but the auxiliary diode D_a is turned on, whereas the freewheeling diodes D_1 and D_2 are still turned off and the resonant diode D_{r1} is still turned off but the resonant diode D_{r2} is still turned on. During this state, the resonant capacitor C_{r1} is still discharged in the opposite direction, and the input inductor currents I_{L1} and I_{L2} charge the capacitors

C_{S1} and C_{S2} of the main switches S_1 and S_2, respectively. As soon as C_{S2} is charged to V_o, this state comes to the end. During this interval, the corresponding state equation can be expressed as follows:

$$\begin{cases} i_{Lr}(t) = -\frac{V_1}{Z_9}\sin\omega_9(t-t_8) - I_1\cos\omega_9(t-t_8) + I_1 - I_{Lr}(t_8) \\ v_{S1}(t) \ = -\frac{C}{C_{S1}}[V_1\cos\omega_9(t-t_8) - I_1 Z_9 \sin\omega_9(t-t_8) - V_1] \\ \qquad\qquad + \frac{I_{L1}}{C_r+C_{S1}}(t-t_8) \\ v_{Cr}(t) = \frac{C}{C_r}\,[V_1\cos\omega_9(t-t_8) - I_1 Z_9 \sin\omega_9(t-t_8) - V_1] \\ \qquad\qquad + \frac{I_{L1}}{C_r+C_{S1}}(t-t_8) + V_{Cr}(t_8) \end{cases} \tag{17}$$

where

$$\begin{aligned} & C = \frac{C_r C_{S1}}{C_r+C_{S1}}, \omega_9 = \sqrt{\frac{1}{L_r C}} = \sqrt{\frac{C_r+C_{S1}}{L_r C_r C_{S1}}} \\ & Z_9 = \sqrt{\frac{L_r}{C}} = \sqrt{\frac{L_r(C_{S1}+C_r)}{C_r C_{S1}}} \\ & V_1 = V_o + V_{Cr}(t_8), I_1 = I_{Lr}\frac{C}{C_{S1}} + I_{L2} + I_{Lr}(t_8) \end{aligned} \tag{18}$$

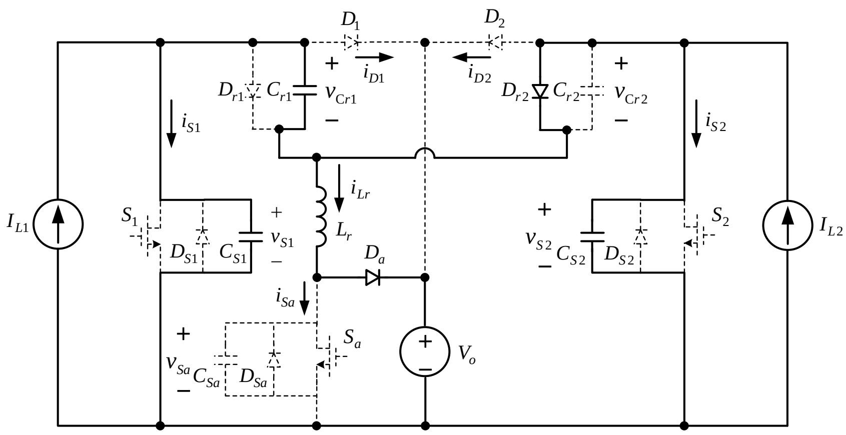

Figure 12. Current flow in state 9.

State 10: $[t_9 \le t \le t_{10}]$. As shown in Figure 13, the main switch S_1 is still turned off and the main switch S_2 is still turned off and the auxiliary switch S_a is still turned off but the auxiliary diode D_a is still turned on, whereas the freewheeling didoes D_1 is still turned off but the freewheeling diode D_2 is turned on but the resonant diode D_{r1} is still turned off but the resonant diode D_{r2} is still turned on. During this state, the voltage across the parasitic capacitor C_{S2} of the main switch S_2 is the input voltage V_o, making D_2 turned on, the auxiliary capacitor C_{r1} is still discharged in the opposite direction, and the parasitic capacitor C_{S1} of the main switch S_1 is still charged. Since D_2, D_{r2}, and D_a are turned on, the voltage across the resonant inductor L_r is zero. The moment C_{S1} reaches V_o, the diode D_1 is turned on, and hence this state comes to the end. During this interval, the corresponding state equation can be signified as follows:

$$\begin{cases} v_{S1}(t) = \frac{I_{L1}}{C_{S1}+C_{r1}}t + v_{S1}(t_9) \\ v_{Cr1}(t) = \frac{I_{L1}}{C_{S1}+C_{r1}}t + v_{S1}(t_9) - V_o \end{cases} \tag{19}$$

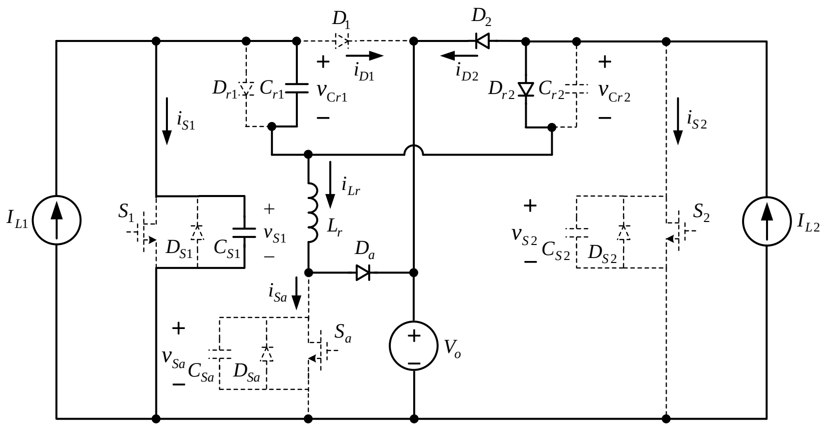

Figure 13. Current flow in state 10.

State 11: $[t_{10} \leq t \leq t_{11}]$. As shown in Figure 14, the main switch S_1 is turned still off and the main switch S_2 is still turned off and the auxiliary switch S_a is still turned off but the auxiliary diode D_a is turned on, whereas the freewheeling didoes D_1 is turned on and the freewheeling diode D_2 is still turned on and the resonant diode D_{r1} is turned on and the resonant diode D_{r2} is still turned on. The instant the auxiliary switch S_a is turned on, this state comes to the end. During this interval, the corresponding state equation can be represented as follows:

$$i_{Lr}(t) = i_{Lr}(t_{10}) \tag{20}$$

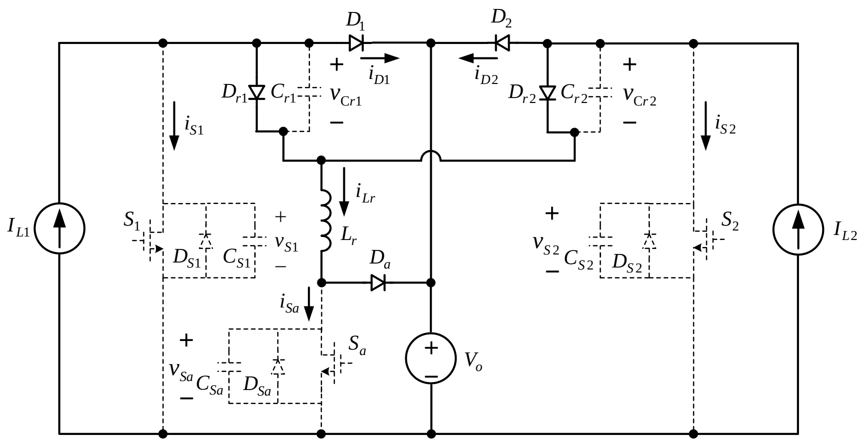

Figure 14. Current flow in state 11.

As the time interval between t_0 and t_{11} is finished, the time interval between t_{11} and t_{21} begins. In other words, the converter enters into the operating states of the second phase. The corresponding operating states are the same as those of the first phase. Eventually, as the time interval between t_{11} and t_{21} is finished, the time comes back to the instant t_0 and the next cycle is repeated.

4. Proposed Control Strategy

Figure 15 shows the proposed control strategy block diagram. First, the output voltage is sensed by a voltage divider with a gain of k. The sensed voltage is sent to the first analog-to-digital converter (ADC1) to obtain the sensed output voltage V_o'. After this, the error coming from V_{ref} minus V_o' is passed to the controller $G_{c1}(z)$ so as to generate a control force. The sensed current after ADC2 is subtracted from this control effort. Therefore, a resulting error is created and sent to the controller $G_{c3}(z)$ so as to yield one pulse-width modulated (PWM) signal after the first PWM generator. This signal will control the main switch of the first phase. On the other hand, the sensed current of the second phase after ADC3, called I'_{L2}, is subtracted from half of the sum of I'_{L1} and I'_{L2}, and the corresponding error is sent to the controller $G_{c2}(z)$ to obtain the other PWM signal after the second PWM generator. This PWM signal is shifted by 180 degrees and then used to drive the main switch of the second phase.

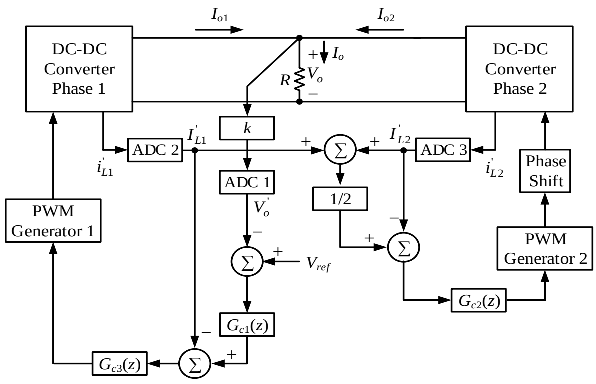

Figure 15. Proposed control block diagram.

The basic operating behavior is described as follows. Since $0.5(I_{L1} + I_{L2})$ is used as the current reference for I_{L2}, the difference between $0.5(I_{L1} + I_{L2})$ and I_{L2} is $0.5(I_{L1} - I_{L2})$ and this value will be sent to the feedback controller such that I_{L1} is almost equal to I_{L2}. On the other hand, $I_{o1} = (1 - D)I_{L1}$ and $I_{o2} = (1 - D)I_{L2}$, where D is a duty cycle. Since $I_{L1} = I_{L2}$ and $I_{o1} = I_{o2} = 0.5I_o$, the current sharing will be achieved.

5. Design of the Key Components

The system specifications of the proposed interleaved boost converter with soft switching can be seen in Table 1, whereas the components used in this converter can be seen in Table 2. The design of the key components is based on Table 1.

Table 1. System specifications of the proposed converter.

System Parameters	Specifications
Operating mode	CCM
Input voltage (V_{in})	24V ± 10%
Output voltage (V_o)	42 V
Rated output current ($I_{o,rated}$)	6 A
Minimum output current ($I_{o,min}$)	0.3 A
Switching frequency (f_s)	25 kHz

Table 2. Components used in the proposed converter.

Components	Specifications
Input Inductor for the first phase (L_1)	720 µH
Input Inductor for the second phase (L_2)	720 µH
Output capacitor (C_o)	680 µF
Resonant inductor (L_r)	6 µH
Resonant capacitor for the first phase (C_{r1})	220 µF
Resonant capacitor for the second phase (C_{r2})	220 µF

5.1. Design of L_1 and L_2

The used converter operates in the continuous conduction mode (CCM) all over the input voltage range and the output current range. The worst case for the design of L_1 is under the minimum input voltage and the minimum output current. It is assumed that as the auxiliary switch is turned on, the voltage across each input inductor is not affected by the resonant inductor. Hence, Figure 16 displays the current in L_1 under the discontinuous conduction mode (BCM), whose direct current (DC) value is I_{LB1}.

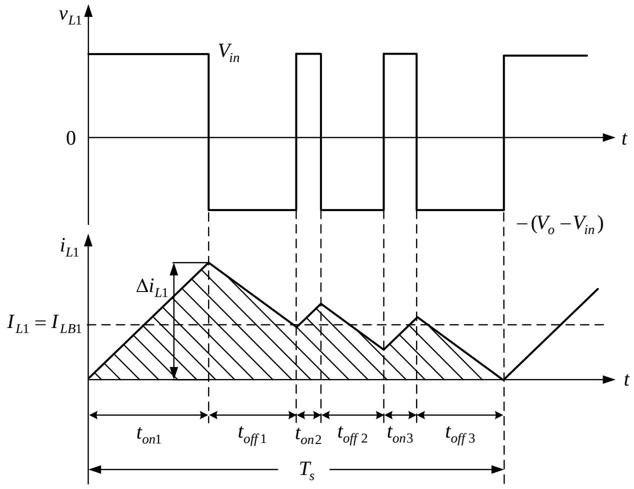

Figure 16. Voltage and current of L_1 under the BCM.

Therefore, based on the following equation, the minimum value of the input inductor, called $L_{1,min}$, can be figured out as below:

$$L_{1,\min} = \frac{V_{in,\min} D_{\max} T_s}{2 \times 0.5 I_{o,\min}} = \frac{V_{in,\min} D_{\max} T_s}{I_{o,\min}} = 699.84 \mu\text{H} \tag{21}$$

Eventually, the value of L_1 is set at 720 µH, which is also for the value of L_2.

5.2. Design of C_o

It is assumed that the voltage ripple is smaller than 0.2% of the output voltage. Since this converter takes a two-phase interleaved structure, the frequency of the output voltage ripple is 50 kHz. Therefore, based on the following equation, the minimum value of the output capacitor, $C_{o,min}$, is as follows:

$$C_{o,\min} = \frac{0.5 I_{o,rated} D_{\max} \times 0.5 T_s}{0.2\% V_o} = \frac{125 I_{o,rated} D_{\max} T_s}{V_o} = 346.43 \mu\text{F} \tag{22}$$

Finally, the value of C_o is set at 680 µH.

5.3. Design of L_r, C_{r1} and C_{r2}

For one PWM cycle, before the main switches S_1 and S_2 are turned off, the auxiliary switch S_a has been turned on so that the main switches S_1 and S_2 will have zero-current transition at turn-off. Since the input voltage locates between 21.6 and 26.4 V, the turn-on time of the main switches locates between 15 and 20 µs. It is assumed that the turn-on time of the auxiliary switch S_a is set to 0.1 times of the turn-on time of the main switches, equal to 1.5 and 2 µs. Hence, the turn-on time of S_a is chosen to be 2 µs, which is the sum of the time intervals of $[t_6, t_7]$ and $[t_7, t_8]$. The resonant current at t_8, called $i_{Lr}(t_8)$, makes the current flowing through the main switch S_1 zero, causing S_1 to be turned on with ZCT. Since $i_{Lr}(t_8) = I_{L1} + I_{L2}$ and $t_8 - t_6 = 2$ µs, based on (13) and (16), the following equation can be obtained as below:

$$(t_8 - t_7) + (t_7 - t_6) = \frac{1}{\omega_8} \sin^{-1}\left(\frac{I_{L1} Z_8}{V_o}\right) + \frac{I_{L2} L_r}{V_o} = 2 \text{ µs} \tag{23}$$

In addition, it is assumed that the resonant period is set at four times of the turn-on time of S_a.

$$f_r = \frac{1}{2\pi\sqrt{L_r C_{r1}}} = 125\text{kHz} \tag{24}$$

From (23) and (24), the value of L_r can be worked out to be 6.7 μH, and the value of C_{r1} can be figured out to be 230 μF. Eventually, the value of L_r is set at 6 μH and the value of C_{r1} is set at 220 μF, which is also for the value of C_{r2}.

In addition, the turn-on time of S_a before the main switches S_1 and S_2 are turned on is set at 1 μs, which is half of the turn-on time of S_a before the main switches S_1 and S_2 are turned off.

6. Experimental Results

Figures 17–27 are measured at the rated load. Figure 17 shows the gate driving signals for S_1, S_2 and S_a, called v_{g1}, v_{g2} and v_{ga}. In addition, v_{g1} and v_{g2} are almost the same except that the difference in phase between them is 180 degrees, and S_a is turned on before S_1 and S_2 are turned on or off. Figure 18 shows the gate driving signal for S_1, called v_{g1}, the voltage across S_1, called v_{S1}, and the current flowing through S_1, called i_{S1}. Figure 19 is the zoom-in of Figure 18 as S_1 is turned on, whereas Figure 20 is the zoom-in of Figure 18 as S_1 is turned off. Figure 21 shows the gate driving signal for S_2, called v_{g2}, the voltage across S_2, called v_{S2}, and the current flowing through S_2, called i_{S2}. Figure 22 is the zoom-in of Figure 21 as S_2 is turned on, whereas Figure 23 is the zoom-in of Figure 21 as S_2 is turned off. Figure 24 displays the gate driving signal for S_a, called v_{ga}, the voltage across S_a, called v_{Sa}, and the current flowing through S_a, called i_{Sa}. Figure 25 is the zoom-in of Figure 24. In addition, Figure 26 shows the voltage across the resonant capacitor C_{r1}, called v_{Cr1}, the voltage across C_{r2}, called v_{Cr2}. Figure 27 displays the voltage across S_1, called v_{S1}, the current in L_1, called i_{L1}, and the current in L_2, called i_{L2}.

From Figures 19 and 20, it can be seen that the main switch S_1 has ZVT turn-on and ZCT turn-off, whereas from Figures 22 and 23, it can be seen that the main switch S_2 has ZVT turn-on and ZCT turn-off. From Figure 25, since the auxiliary switch S_a is connected in series with the resonant inductor L_r, thereby making i_{Sa} increase slowly and hence causing S_a to be turned on with ZCS. From Figure 26, via C_{r1}, C_{r2}, and L_r in the resonant loop along with C_{S1} and C_{S2} of the main switches S_1 and S_2, the soft switching of the main switches for individual phases can be realized. It is noted that due to the diode clamp, C_{r1} and C_{r2} can be reversely charged to $-V_o$. From Figure 27, it can be seen that the DC values of i_{L1} and i_{L2} are almost the same, and i_{L2} is shifted from i_{L1} by 180 degrees.

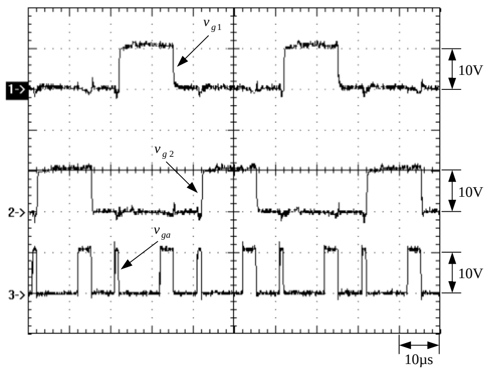

Figure 17. Gate driving signals: (1) v_{g1}; (2) v_{g2}; (3) v_{ga}.

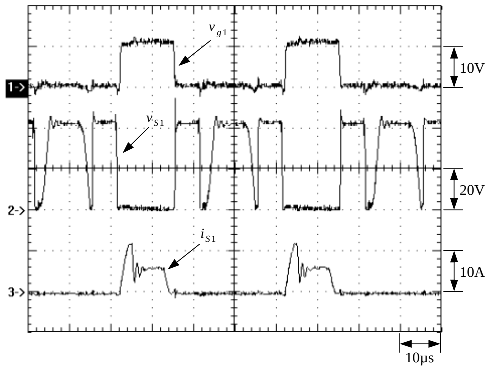

Figure 18. Waveforms relevant to S_1: (1) v_{g1}; (2) v_{S2}; (3) i_{S1}.

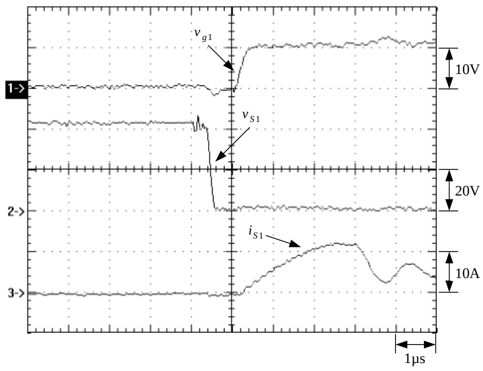

Figure 19. Zoom-in of Figure 17 as S_1 is turned on: (1) v_{g1}; (2) v_{S1}; (3) i_{S1}.

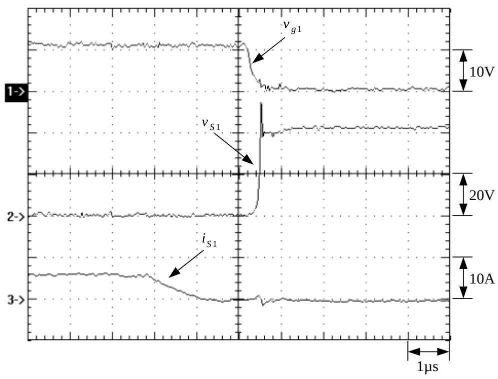

Figure 20. Zoom-in of Figure 17 as S_1 is turned off: (1) v_{g1}; (2) v_{S1}; (3) i_{S1}.

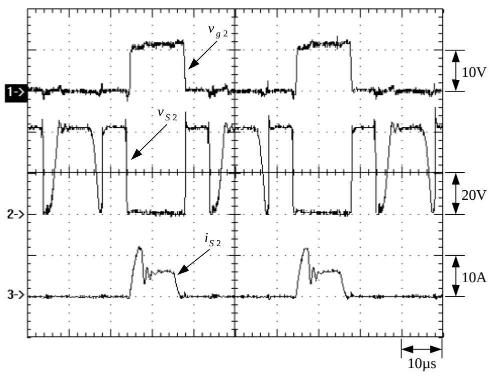

Figure 21. Waveforms relevant to S_2: (1) v_{g2}; (2) v_{S2}; (3) i_{S2}.

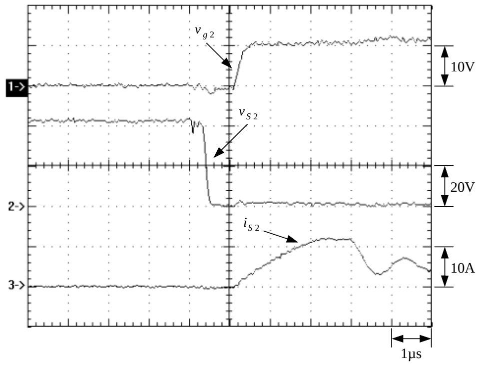

Figure 22. Zoom-in of Figure 20 as S_2 is turned on: (1) v_{g2}; (2) v_{S2}; (3) i_{S2}.

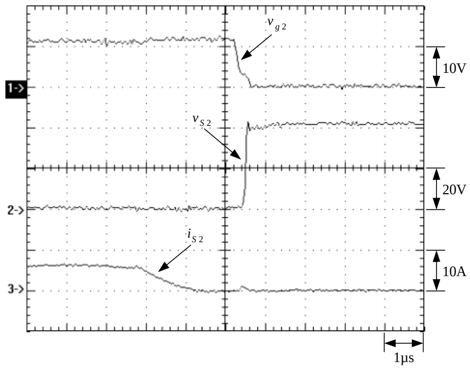

Figure 23. Zoom-in of Figure 20 as S_2 is turned off: (1) v_{g2}; (2) v_{S2}; (3) i_{S2}.

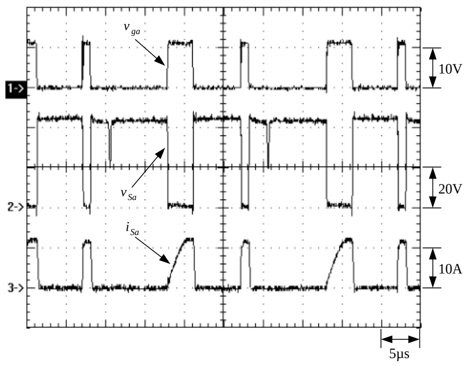

Figure 24. Waveforms relevant to S_a: (1) v_{ga}; (2) v_{Sa}; (3) i_{Sa}.

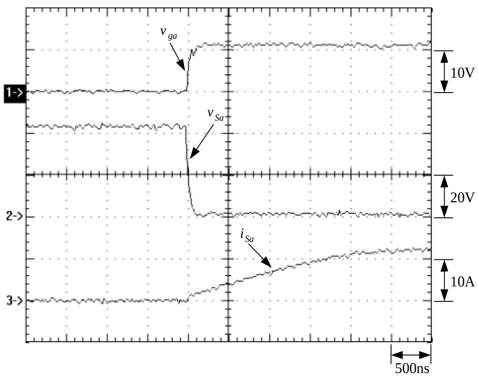

Figure 25. Zoom-in of Figure 23 as S_a is turned on: (1) v_{ga}; (2) v_{Sa}; (3) i_{Sa}.

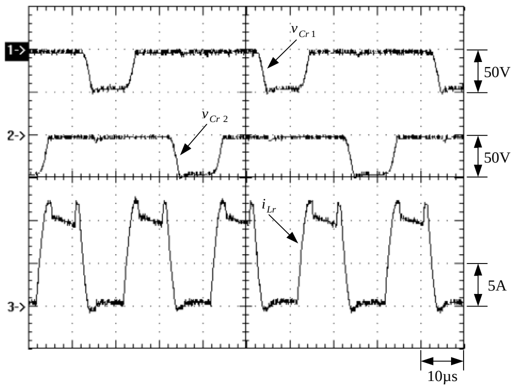

Figure 26. Waveforms relevant to the resonant loop: (1) v_{Cr1}; (2) v_{Cr2}; (3) i_{Lr}.

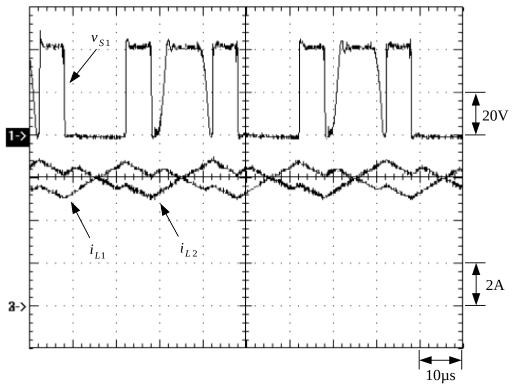

Figure 27. Waveforms relevant to current sharing: (1) v_{S1}; (2) i_{L1}; (3) i_{L2}.

On the other hand, Figure 28 shows how to measure the efficiency. First of all, as displayed in Figure 28, the input current I_{in} is attained by measuring the voltage across the current-sensing resistor according to the digital meter named Fluke 8050 A. Next, the input voltage V_{in} is obtained also by the digital meter. Therefore, the input power is the product of V_{in} and I_{in}. Concerning the output power, the output current I_o is read from the electronic load and the output voltage V_o is attained also by the digital meter. Hence, the output power can be gotten. Eventually, the accompanying efficiency can be attained. Figure 29 displays the curves of efficiency versus load under the input voltage of 24 V. From Figure 29, it can be seen that the converter with the proposed soft switching circuit has higher efficiency than that of the converter without the proposed soft switching circuit. Particularly, the difference in efficiency between with and without the proposed soft switching can be up to about 9%, which occurs at minimum load.

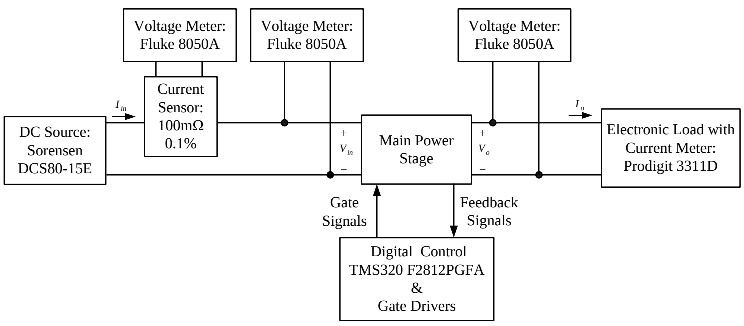

Figure 28. Efficiency measurement block diagram.

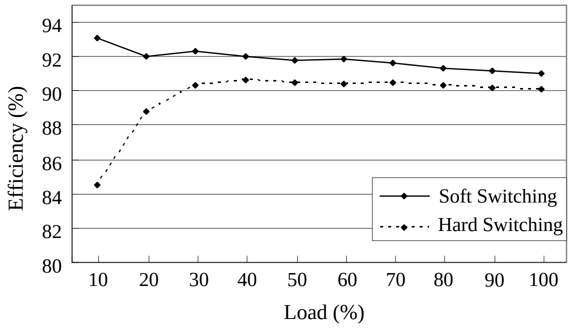

Figure 29. Curves of efficiency versus load under the input voltage of 24 V.

7. Conclusions

A soft switching method is presented herein, which is applied to a two-phase interleaved boost converter. The concept of this method is that the auxiliary switch S_a is turned on before the main switches S_1 and S_2 are turned on/off. By doing so, the ZVT turn-on and ZCT-turn-off of S_1 and S_2 can be achieved, leading to improvement in the overall efficiency. Furthermore, two phases use the same resonant inductor such that the circuit size can be reduced. In addition, S_a is turned on with ZCS due to S_a and L_r being connected in series.

Author Contributions: Conceptualization, K.-I.H.; methodology, K.-I.H.; software, W.-Z.J.; validation, W.-Z.J.; formal analysis, W.-Z.J.; investigation, J.-J.S.; resources, K.-I.H.; data curation, J.-J.S.; writing—original draft preparation, K.-I.H.; writing—review and editing, K.-I.H.; visualization, J.-J.S.; supervision, K.-I.H.; project administration, K.-I.H.; funding acquisition, K.-I.H. All authors have read and agreed to the published version of the manuscript.

Funding: This research was funded by the Ministry of Science and Technology, Taiwan, under the Grant Number: MOST 108-2221-E-027-051.

Acknowledgments: The authors gratefully acknowledge the support of the Ministry of Science and Technology, Taiwan, under the Grant Number MOST 108-2221-E-027-051.

Conflicts of Interest: The authors declare no conflict of interest with commerce.

References

1. Lee, F.C. High-frequency quasi-resonant and multi-resonant converter technologies. In Proceedings of the 14 Annual Conference of Industrial Electronics Society, Singapore, 24–28 October 1988; pp. 509–521.
2. Chuang, Y.; Ke, Y. A novel high-efficiency battery charger with a buck zero-voltage-switching resonant converter. *IEEE Trans. Energy Convers.* **2007**, *22*, 848–854. [CrossRef]
3. Mousavi, A.; Das, P.; Moschopoulos, G. A comparative study of a New ZCS DC-DC full-bridge boost converter with a ZVS active-clamp converter. *IEEE Trans. Power Electron.* **2012**, *27*, 1347–1358. [CrossRef]
4. Ge, T.; Carpenter, B.; Ngo, K.D.T. Resonant cross-commutated Dc-Dc converter. *IEEE Trans. Ind. Electron.* **2017**, *64*, 8782–8785. [CrossRef]
5. Hong, J.; Deng, X.; Zhang, G.; Huang, Z.; Li, X.; Zhang, Y. Sneak circuit identification of an improved boost converter with soft-switching realization. *IEEE J. Emerg. Sel. Top. Power Electron.* **2019**, *7*, 2394–2402. [CrossRef]
6. Lin, B.; Hsieh, F. Soft-switching zeta-flyback converter with a buck-boost type of active clamp. *IEEE Trans. Ind. Electron.* **2007**, *54*, 2813–2822.
7. Han, S.K.; Yoon, H.K.; Moon, G.W.; Youn, M.J.; Kim, Y.H.; Lee, K.H. A new active clamping zero-voltage switching PWM current-fed half-bridge converter. *IEEE Trans. Power Electron.* **2005**, *20*, 1271–1279. [CrossRef]
8. Lee, Y.; Lin, B. Adding active clamping and soft switching to boost-flyback single-stage isolated power-factor-corrected power supplies. *IEEE Trans. Power Electron.* **1997**, *12*, 1017–1027.
9. Watson, R.; Hua, G.C.; Lee, F.C. Characterization of an active clamp flyback topology for power factor correction applications. *IEEE Trans. Power Electron.* **1996**, *11*, 191–198. [CrossRef]

10. Tuomainen, V.; Kyyra, J. Effect of resonant transition on efficiency of forward converter with active clamp and self-driven SRs. *IEEE Trans. Power Electron.* **2005**, *20*, 315–323. [CrossRef]
11. Zhao, Q.; Lee, F.C. High-efficiency, high step-up DC-DC converters. *IEEE Trans. Power Electron.* **2003**, *18*, 65–73. [CrossRef]
12. Lin, B.-R.; Huang, C.E.; Wang, D. Analysis and implementation of a zero-voltage switching forward converter with a synchronous rectifier. *IEE Proc. Electr. Power Appl.* **2005**, *152*, 1085–1092. [CrossRef]
13. Lo, Y.; Lin, J. Active-clamping ZVS flyback converter employing two transformers. *IEEE Trans. Power Electron.* **2007**, *22*, 2416–2423. [CrossRef]
14. Watson, R.; Lee, F.C.; Hua, G.C. Utilization of an active-clamp circuit to achieve soft switching in flyback converters. *IEEE Trans. Power Electron.* **1996**, *11*, 162–169. [CrossRef]
15. Wu, T.; Lai, Y.; Hung, J.; Chen, Y. Boost converter with coupled inductors and buck-boost type of active clamp. *IEEE Trans. Ind. Electron.* **2008**, *55*, 154–162. [CrossRef]
16. Xinke, W.; Junming, Z.; Xin, Y.; Zhaoming, Q. Analysis and design for a new ZVS DC-DC converter with active clamping. *IEEE Trans. Power Electron.* **2006**, *21*, 1572–1579.
17. Suryawanshi, H.M.; Ramteke, M.R.; Thakre, K.L.; Borghate, V.B. Unity-power-factor operation of three-phase AC-DC soft switched converter based on boost active clamp topology in modular approach. *IEEE Trans. Power Electron.* **2008**, *23*, 229–236. [CrossRef]
18. Duarte, C.M.C.; Fiori, V.M. A new ZVS-PWM active-clamping buck-boost converter. In Proceedings of the IEEE PESC'05, Recife, Brazil, 16–16 June 2005; pp. 1429–1433.
19. Ma, Y.; Wu, X.; Xie, X.; Chen, G.; Qian, Z. A new ZVS-PWM buck converter with an active camping cell. In Proceedings of the IEEE IECON'07, Taipei, Taiwan, 5–8 November 2007; pp. 1592–1597.
20. Lin, B.; Huang, C.; Chiang, H. Analysis of a soft switching PWM active clamp Cuk converter. In Proceedings of the IEEE ICIEA'07, Harbin, China, 23–25 May 2007; pp. 2311–2316.
21. Tseng, C.; Chen, C. A novel ZVT PWM Cuk power-factor corrector. *IEEE Trans. Ind. Electron.* **1999**, *46*, 780–787. [CrossRef]
22. Hua, G.; Leu, C.; Jiang, Y.; Lee, F.C.Y. Novel zero-voltage-transition PWM converters. *IEEE Trans. Power Electron.* **1994**, *9*, 213–219.
23. Tseng, C.; Chen, C. Novel ZVT-PWM converters with active snubbers. *IEEE Trans. Power Electron.* **1998**, *13*, 861–869. [CrossRef]
24. Cho, J.; Baek, J.; Yoo, D.; Lee, H. Reduced conduction loss zero-voltage-transition power factor correction converter with low cost. *IEEE Trans. Ind. Electron.* **1998**, *45*, 395–400.
25. Martins, M.L.d.S.; Hey, H.L. Self-commutated auxiliary circuit ZVT PWM converters. *IEEE Trans. Power Electron.* **2004**, *19*, 1435–1445. [CrossRef]
26. Li, W.; He, X. ZVT interleaved boost converters for high-efficiency, high step-up DC-DC conversion. *IET Electr. Power Appl.* **2007**, *1*, 284–290. [CrossRef]
27. Wang, D.; He, X.; Zhao, R. ZVT interleaved boost converters with built-in voltage doubler and current auto-balance characteristic. *IEEE Trans. Power Electron.* **2008**, *23*, 2847–2854. [CrossRef]
28. Das, P.; Moschopoulos, G. A comparative study of zero-current-transition PWM converters. *IEEE Trans. Ind. Electron.* **2007**, *54*, 1319–1328. [CrossRef]
29. Bodur, H.; Bakan, A.F. An improved ZCT-PWM DC-DC converter for high-power and frequency applications. *IEEE Trans. Ind. Electron.* **2004**, *51*, 89–98. [CrossRef]
30. Adib, E.; Farzaneh-fard, H. New zero current transition PWM converters. In Proceedings of the IEEE ICIT'06, Mumbai, India, 15–17 December 2006; pp. 2131–2136.
31. Duarte, C.M.C.; Barbi, I. A family of ZVS-PWM active-clamping DC-to-DC converters: Synthesis, analysis, design, and experimentation. *IEEE Trans. Circuits Syst. I Fundam. Theory Appl.* **1997**, *44*, 698–704. [CrossRef]
32. Kumar, A.P.; Subrahmanya Kumar Bhajana, V.V.; Drabek, P. A novel ZVT/ZCT bidirectional DC-DC converter for energy storage applications. In Proceedings of the IEEE SPEEDAM'16, Anacapri, Italy, 22–24 June 2016; pp. 979–983.
33. De, O.; Stein, C.M.; Hey, H.L. A true ZCZVT commutation cell for PWM converters. *IEEE Trans. Power Electron.* **2000**, *15*, 185–193.
34. Hu, Z.; Zhang, B.; Deng, W. Study on novel ZVZCT PWM DC-DC converter family. In Proceedings of the IEEE IPEMC'04, Xi'an, China, 14–16 August 2004; pp. 154–159.

35. Cho, J.; Baek, J.; Rim, G.; Kang, I. Novel zero-voltage-transition PWM multiphase converters. *IEEE Trans. Power Electron.* **1998**, *13*, 152–159.
36. Tseng, S.-Y.; Shiang, J.-Z.; Chang, H.H.; Jwo, W.-S.; Hsieh, C.-T. A novel turn-on/off snubber for interleaved boost converters. In Proceedings of the IEEE PESC'07, Qrlando, FL, USA, 17–21 June 2007; pp. 2341–2347.
37. Hwu, K.I.; Tu, W.C.; Hon, M.J. A dimmable LED driver based on current balancing transformer with magnetizing energy recycling considered. *IEEE J. Display Technol.* **2014**, *10*, 388–395. [CrossRef]
38. Hwu, K.I.; Jiang, W.Z.; Hsiao, C.W. Dimmable LED driver based on twin-bus converter and differential-mode transformer. *IEEE J. Disp. Technol.* **2016**, *12*, 1122–1129. [CrossRef]
39. Qu, X.; Wong, S.C.; Chi, K.T. An improved LCLC current-source-output multistring LED driver with capacitive current balancing. *IEEE Trans. Power Electron.* **2015**, *30*, 5783–5791. [CrossRef]
40. Ye, Y.; Eric Cheng, K.W.; Lin, J.; Wang, D. Single-switch multichannel current-balancing LED drive circuits based on optimized SC techniques. *IEEE Trans. Ind. Electron.* **2015**, *62*, 4761–4768. [CrossRef]
41. Chiub, C.; Chen, K. A high accuracy current-balanced control technique for LED backlight. In Proceedings of the IEEE PESC'08, Rhodes, Greece, 15–19 June 2008; pp. 4202–4206.
42. Yu, W.; Lai, J.; Ma, H.; Zheng, C. High-Efficiency dc-dc converter with twin bus for dimmable LED lighting. *IEEE Trans. Power Electron.* **2011**, *26*, 2095–2100. [CrossRef]
43. Lohaus, L.; Liao, L.; Strache, S.; Wunderlich, R.; Heinen, S. Energy efficient current control technique for driving high power LEDs. In Proceedings of the VDE PRIME'12, Aachen, Germany, 12–15 June 2012; pp. 75–78.
44. Li, S.N.; Zhong, W.X.; Chen, W.; Hui, R.S.Y. Novel self-configurable current-mirror techniques for reducing current imbalance in parallel light-emitting diode (LED) strings. *IEEE Trans. Power Electron.* **2012**, *27*, 2153–2162. [CrossRef]
45. Li, Y.; Chen, C. A novel primary-side regulation scheme for single-stage high-power-factor ac-dc LED driving circuit. *IEEE Trans. Ind. Electron.* **2013**, *60*, 4978–4986. [CrossRef]